J|A|C|S
ARTICLES
Published on Web 04/05/2002

Self-Assembled, Helically Stacked Anionic Aggregates of 2,5,8,11-Tetra-*tert*-butylcycloocta[1,2,3,4-*def*;5,6,7,8-*d′e′f′*]bisbiphenylene, Stabilized by Electrostatic Interactions

Roy Shenhar,[†] Hua Wang,[‡] Roy E. Hoffman,[†] Limor Frish,[§] Liat Avram,[§] Itamar Willner,[†] Andrzej Rajca,[‡] and Mordecai Rabinovitz*,[†]

Contribution from the Department of Organic Chemistry, Safra Campus, The Hebrew University of Jerusalem, Givat Ram, Jerusalem 91904, Israel, Department of Chemistry, University of Nebraska, Lincoln, Nebraska 68588-0304, and School of Chemistry, The Sackler Faculty of Exact Sciences, Tel Aviv University, Ramat Aviv, Tel Aviv 69978, Israel

Received September 4, 2001

Abstract: Tetraanions of alkyl-substituted derivatives of cycloocta[1,2,3,4-*def*;5,6,7,8-*d′e′f′*]bisbiphenylene (BPD) and their counter lithium cations self-assemble to form helically stacked assemblies, including a dimer, a trimer, and a tetramer. NMR self-diffusion measurements and unprecedented magnetic shielding effects for the sandwiched lithium cations support their aggregated nature. The D_2-tetramer assembly is fully characterized by NMR spectroscopy, providing unequivocal evidence for a helix of four tetraanionic BPD layers with an estimated relative twist angle of about 45° and interlayer spacing of ca. 4 Å. The barrier for racemization through the in-plane inter-deck rotation is $\Delta G_{200}^{\ddagger} = 9.5 \pm 0.2$ kcal mol^{-1} in the dimer compared to >15 kcal mol^{-1} in the tetramer.

Introduction

Inspired by nature, where helical structures play a major motif for recognition, replication, and catalysis, chemists are challenged in tailoring synthetic self-organized helical assemblies that exhibit unique recognition[1] or catalytic properties[1a,2] and nonlinear features.[3] Various self-assembly methods including the use of hydrogen bonding[4] and ordered metal ligation[5] were reported to form helical supramolecular structures. Also, the organization of discotic molecular components in a columnar stacking[6] that includes a progressive helical twist between adjacent layers leads to the formation of helical superstructures. Planar molecules (sometimes as planar hydrogen bonded assemblies[4d,7,8]) with appropriate peripheral substituents[3b,7,9] are used as building blocks, while π-stacking,[3,8,9] metal coordination,[6d,9b] and charge-transfer interactions[10] are the driving interactions for the formation of helical assemblies.

Alkali metal cations are also capable of attracting several negative organic ions to form aggregates.[11] Stacked assemblies can result from the electrostatic interaction between alkali metal cations and highly charged polycyclic aromatic hydrocarbons (PAHs), which are capable of bearing high negative charge due to extended π-conjugation.[12] Since the overall electrostatic

* Address correspondence to this author. E-mail: mordecai@vms.huji.ac.il.
[†] The Hebrew University of Jerusalem.
[‡] University of Nebraska.
[§] Tel Aviv University.

(1) (a) Lehn, J.-M. *Angew. Chem., Int. Ed. Engl.* **1990**, *29*, 1304−1319. (b) Rivera, J. M.; Martín, T.; Rebek, J., Jr. *Science* **1998**, *279*, 1021−1023. (c) Nakano, T.; Satoh, Y.; Okamoto, Y. *Macromolecules* **2001**, *34*, 2405−2407. (d) Nakano, T.; Ueda, K.; Okamoto, Y. *J. Polym. Sci. Part A.: Polym. Chem.* **2001**, *39*, 1610−1614. (e) Liu, Y.; You, C. C.; Wada, T.; Inoue Y. *J. Org. Chem.* **1999**, *64*, 3630−3634. (f) Jodry, J. J.; Lacour, J. *Chem. Eur. J.* **2000**, *6*, 4297−4304. (g) Nakagawa, H.; Gomi, K.; Yamada, K. *Chem. Pharm. Bull.* **2001**, *49*, 49−53. (h) Castellano, R. K.; Nuckolls, C.; Rebek, J., Jr. *J. Am. Chem.* **1999**, *121*, 11156−11163 and references therein. (i) Green, M. M.; Peterson, N. C.; Sato, T.; Teramoto, A.; Cook, R.; Lifson, S. *Science* **1995**, *268*, 1860−1866. (j) Furusho, Y.; Kimura, T.; Mizuno, Y.; Aida, T. *J. Am. Chem. Soc.* **1997**, *119*, 5267−5268.
(2) See, for example: (a) Willner, I.; Heleg-Shabtai, V.; Katz, E.; Rau, H. K.; Haehnel, W. *J. Am. Chem. Soc.* **1999**, *121*, 6455−6468. (b) Strong, A. E.; Moore, B. D. *J. Mater. Chem.* **1999**, *9*, 1095−1105.
(3) (a) Verbiest, T.; van Elshocht, S.; Kauranen, M.; Hellemans, L.; Snauwaert, J.; Nuckolls, C.; Katz, T. J.; Persoons, A. *Science* **1998**, *282*, 913−915. (b) Fox, J. M.; Katz, T. J.; van Elshocht, S.; Verbiest, T.; Kauranen, M.; Persoons A.; Thongpanchang, T.; Krauss, T.; Brus, L. *J. Am. Chem. Soc.* **1999**, *121*, 3453−3459.
(4) (a) Piguet, C.; Bernardinelli, G.; Hopfgartner, G. *Chem. Rev.* **1997**, *97*, 2005−2062 and references therein. (b) Suárez, M.; Branda, N.; Lehn, J.-M.; Decian, A.; Fischer, J. *Helv. Chim. Acta* **1998**, *81*, 1−13. (c) Lehn, J.-M. *Supramolecular Chemistry, Concepts and Perspectives*; VCH: Weinheim, Germany, 1995. (d) Whitesides, G. M.; Mathias, J. P.; Seto, C. T. *Science* **1991**, *254*, 1312−1319. (e) Whitesides, G. M.; Simanek, E. E.; Mathias, J. P.; Seto, C. T.; Chin, D. N.; Mammen, M.; Gordon, D. M. *Acc. Chem. Res.* **1995**, *28*, 37−44.
(5) See, for example: (a) Baum, G.; Constable, E. C.; Fenske, D.; Housecroft, C. E.; Kulke, T.; Neuburger, M.; Zehnder, M. *J. Chem. Soc., Dalton. Trans.* **2000**, 945−959. (b) Smith, V. C. M.; Lehn, J.-M. *Chem. Commun.* **1996**, 2733−2734.
(6) See, for example: (a) Schmidt-Mende, L.; Fechtenkotter, A.; Müllen, K.; Moons, E.; Friend, R. H.; MacKenzie, J. D. *Science* **2001**, *293*, 1119−1122. (b) Brand, J. D.; Kubel, C.; Ito, S.; Müllen, K. *Chem. Mater.* **2000**, *12*, 1638−1647. (c) Andersen, T. L.; Krebs, F. C.; Thorup, N.; Bechgaard, K. *Chem. Mater.* **2000**, *12*, 2428−2433. (d) Ohta, K.; Inagaki-Oka, Y.; Hasebe, H.; Yamamoto, I. *Polyhedron* **2000**, *19*, 267−274.
(7) (a) Jolliffe, K. A.; Timmerman, P.; Reinhoudt, D. N. *Angew. Chem., Int. Ed. Engl.* **1999**, *38*, 933−937. (b) Prins, L. J.; Huskens, J.; de Jong, F.; Timmerman, P.; Reinhoudt, D. N. *Nature* **1999**, *398*, 498−502. (c) Prins, L. J.; de Jong, F.; Timmerman, P.; Reinhoudt, D. N. *Nature* **2000**, *408*, 181−184.
(8) (a) Hirschberg, J. H. K. K.; Brunsveld, L.; Ramzi, A.; Vekemans, J. A. J. M.; Sijbesma, R. P.; Meijer, E. W. *Nature* **2000**, *407*, 167−170. (b) Palmans, A. R. A.; Vekemans, J. A. J. M.; Havinga, E. E.; Meijer, E. W. *Angew. Chem., Int. Ed. Engl.* **1997**, *36*, 2648−2651.
(9) (a) Fechtenkotter, A.; Tchebotareva, N.; Watson, M.; Müllen. K. *Tetrahedron* **2001**, *57*, 3769−3783. (b) Engelkamp, H.; Middelbeek, S.; Nolte, R. J. M. *Science*, **1999**, *284*, 785−788.
(10) Gallivan, J. P.; Schuster, G. B. *J. Org. Chem.* **1995**, *60*, 2423−2429.
(11) (a) Bock, H.; Gharagozloo-Hubmann, K.; Sievert, M.; Prisner, T.; Havlas, Z. *Nature* **2000**, *404*, 267−269. (b) Günther, H. *J. Braz. Chem. Soc.* **1999**, *10*, 241−262.

interaction between reduced PAHs and alkali metal cations increases quadratically with the degree of reduction, the tendency of some PAHs to aggregate is reflected only at highly reduced states. A representative example is the tetralithio tetraanion of corannulene (the smallest bowl-shaped subunit of C_{60}), which exhibits a stacked dimer structure in tetrahydrofuran (THF) solution.[13] To our knowledge, higher order aggregates in which multiple lithium cations link more than two PAH polyanions to form stable *soluble* sandwich aggregates have not been reported, as most charged PAHs that do aggregate tend to precipitate.[11a] There is, however, evidence that an alkyl-substituted biphenylene, namely octamethylbiphenylene, forms soluble aggregates upon reduction to a dianion with lithium, though their structures are not known.[12c]

Herein we describe the preparation and complete structural characterization of an unusual helical tetramer aggregate, in which four tetraanions of a cycloocta[1,2,3,4-*def*;5,6,7,8-*d′e′f′*]-bisbiphenylene derivative form a soluble, helically stacked assemmbly with lithium cations.

Results and Discussion

Cycloocta[1,2,3,4-*def*;5,6,7,8-*d′e′f′*]bisbiphenylene (**1**, a biphenylene dimer, termed BPD) is an almost planar, highly symmetrical PAH.[14] Earlier studies on the reduction of its tetra-*tert*-butyl derivative (**2**) revealed the formation of the respective radical anion and dianion ($\mathbf{2}^{2-}$).[14] Further reduction of $\mathbf{2}^{2-}$ at low temperature gives rise to three new species identified as aggregates of the tetraanion $\mathbf{2}^{4-}$: dimer of $\mathbf{2}^{4-}$, trimer of $\mathbf{2}^{4-}$, and tetramer of $\mathbf{2}^{4-}$. We shall first focus on the structure elucidation and characteristics of the dimer and the tetramer.

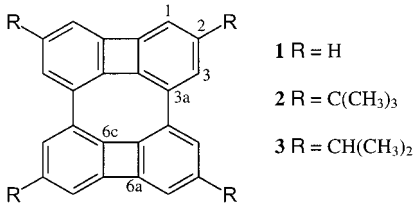

1 R = H

2 R = $C(CH_3)_3$

3 R = $CH(CH_3)_2$

Helically Stacked Dimer of $\mathbf{2}^{4-}$. The first new species formed is assigned to a dimer of $\mathbf{2}^{4-}$ (accompanied by a small amount of higher oligomers). The ^{1}H NMR spectrum of the dimer of $\mathbf{2}^{4-}$ at 260 K is analogous to that of the dianion, i.e., two resonances for the aromatic protons and one resonance for the *tert*-butyl protons (Figure 1A). The high symmetry reflected in the simple spectrum of the dimer disguises it as a monomer.[13] At lower temperatures (180 K), the spectral pattern of the ^{1}H and ^{13}C NMR spectra of the dimer of $\mathbf{2}^{4-}$ is split into two sets (Figure 2). Complete assignment of its low-temperature NMR spectra, including NOE experiments, supports a helically stacked structure of two tetraanionic decks, in which the symmetry across the bays is broken. Furthermore, analogous lithium reduction of a tetraisopropyl derivative of BPD (**3**) to the corresponding tetraanion $\mathbf{3}^{4-}$ gives a dimer of $\mathbf{3}^{4-}$, in which

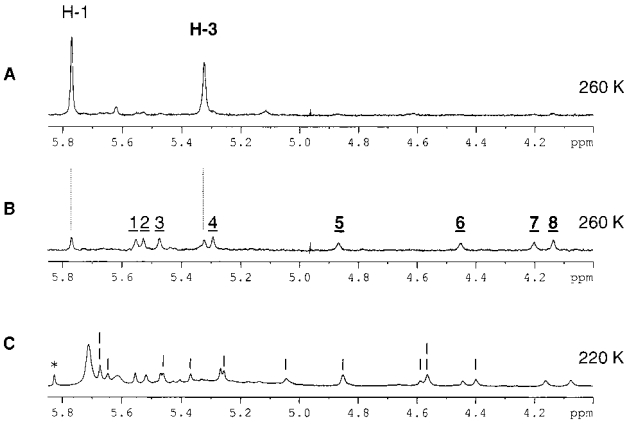

Figure 1. Low-field portion of the ^{1}H NMR spectra, showing the aromatic biphenyl-type bay protons (boldface labels) and biphenylene-type bay proton peaks. (A) $\mathbf{2}^{4-}$ dimer (with traces of the tetramer). (B) $\mathbf{2}^{4-}$ dimer and tetramer (after warming to room temperature). The eight "aromatic" peaks of the tetramer of $\mathbf{2}^{4-}$ are numbered (underlined). (C) Dimer, trimer, and tetramer of $\mathbf{2}^{4-}$. Twelve short segments denote the trimer signals. An asterisk denotes the H-1 peak of $\mathbf{2}^{2-}$. All other peaks are attributed to the dimer and tetramer (the missing peak for H-3 of the dimer is due to coalescence).

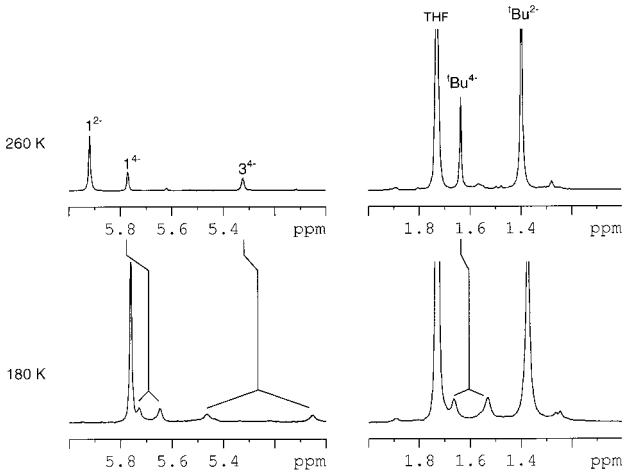

Figure 2. Variable-temperature experiment on a mixture of a dianion and a tetraanion dimer of **2**, showing the splitting of all three peaks of the tetraanionic dimer at low temperatures. The superscript inscription denotes the reduction state of the referred species which peak is labeled.

the methyl groups in each isopropyl substituent are diastereotopic, giving rise to *two* doublet proton resonances (Figure 3).[15] The above evidence is consistent with a dimer in which two helically stacked tetraanionic decks rotate in plane, and this rotation is inhibited at low temperatures. The energy barrier calculated for this in-plane rotation, corresponding to an interconversion of enantiomers of the dimer, is $\Delta G_{200}^{\ddagger} = 9.5 \pm 0.2$ kcal mol^{-1}.

Helically Stacked Structure of a Tetramer of $\mathbf{2}^{4-}$. Even more interesting is the formation of a further stabilized species derived from $\mathbf{2}^{4-}$ dimer that is attributed to a different type of $\mathbf{2}^{4-}$ aggregate. This aggregate is spontaneously formed at a low temperature, and its formation can be accelerated by elevating the sample temperature to 298 K.[16] For simplicity we shall use the underlined notation appearing in Figure 1B for the description of the NMR spectra interpretation. The resulting ^{1}H NMR spectrum exhibits an apparent 4-fold multiplication of the

(12) (a) Paquette, L. A.; Bauer, W.; Sivik, M. R.; Bühl, M.; Fiegel, M.; Schleyer, P. v. R. *J. Am. Chem. Soc.* **1990**, *112*, 8776−8789. (b) Eiermann, M.; Hafner, K. *J. Am. Chem. Soc.* **1992**, *114*, 135−140. (c) Bausch, J. W.; Gregory, P. S.; Olah, G. A.; Prakash, G. K. S.; Schleyer, P. v. R.; Segal, G. A. *J. Am. Chem. Soc.* **1989**, *111*, 3633−3640.

(13) Ayalon, A.; Sygula, A.; Cheng, P.-C.; Rabinovitz, M.; Rabideau, P. W.; Scott, L. T. *Science* **1994**, *265*, 1065−1067.

(14) Rajca, A.; Safronov, A.; Rajca, S.; Ross, C. R., II; Stezowski, J. J. *J. Am. Chem. Soc.* **1996**, *118*, 7272−7279.

(15) The NMR characteristics (especially the ^{7}Li NMR) of the tetraanion aggregates of **3** suggest that these aggregates are tighter than the aggregates of $\mathbf{2}^{4-}$ (to be published).

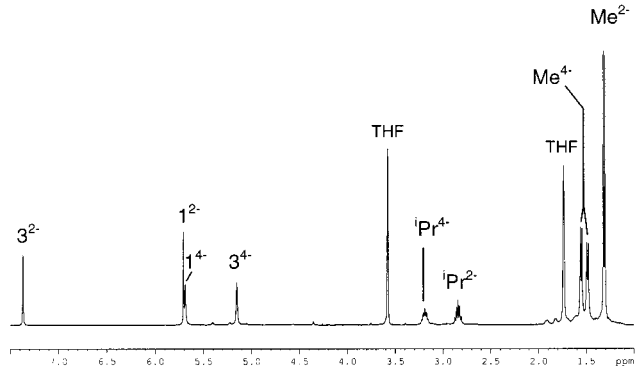

Figure 3. ^{1}H NMR spectrum (at 250 K) of a mixture of a dianion and a tetraanion dimer of **3**, showing the duplication of the methyl groups doublet into two resonances in the tetraanion dimer. The superscript inscription denotes the reduction state of the referred species which peak is labeled.

spectral pattern (vs the parent compound), showing eight aromatic and four *tert*-butyl resonances. (Analogous behavior is found in the ^{13}C NMR spectrum.) This spectral complexity is not likely to implicate distorted conformations as the NMR spectra do not show any signs of coalescence even at relatively high temperatures (e.g., 298 K), which indicates a high barrier (>15 kcal mol^{-1}) for any dynamic process to take place. The BPD skeleton appears intact and tetraanionic as indicated by the following data: (a) all eight "aromatic" protons[17] exhibit *singlet* resonances and are attached to π-skeleton carbons that retain their sp^2 hybridization,[18] precluding protonation on most of the π-skeleton carbons, (b) a reaction with oxygen yields **2**, (c) addition of an equivalent amount of **2** to a solution dominated by the new species quantitatively regenerates the dianion **2**$^{2-}$, as monitored by ^{1}H NMR (Supporting Information, Figure S9), and (d) UV−vis-monitored titration of a solution dominated by the new species with **2** gives isosbestic points between the new species and the dianion of **2** (Supporting Information, Figure S10).

Very weak through-bond correlations are observed in the COSY spectrum [enhanced in the total correlation spectroscopy (TOCSY) spectrum,[19] Figure 4], which distinguish four pairs of peaks: 1-5, 2-8, 3-7, and 4-6. It should be noted that one of each pair of peaks belongs to the group appearing at low field (1,2,3,4), while the other resonance belongs to the more shielded group (5,6,7,8). These through-bond correlations are attributed to *meta* couplings,[20] which means that each pair of protons resides on *the same* aromatic ring. This finding is further supported by the long-range ^{13}C−^{1}H correlation experiment,[21] as each proton correlates to its counterpart's attached carbon, which is located three bonds away (e.g. H-3 correlates to C-7, and H-7 correlates to C-3, etc.).

(16) Warming to room temperature is only used to accelerate the tetramerization process, which occurs also at lower temperatures. Using this method of straightforward conversion of the dimer to the tetramer by warming to room temperature and following the changes in the ^{7}Li NMR spectrum probably affords the best way to assign the ^{7}Li NMR peaks of both species.

(17) For simplicity, we shall continue the use of the term "aromatic protons" to denote the protons attached to the π-skeleton even in the anions, although the aromatic nature of the system in the reduced states is not clear.

(18) The ^{13}C−^{1}H coupling constant values measured for the aromatic protons are ~150 Hz, which is indicative of sp^2 hybridization.

(19) A TOCSY experiment reveals through-bond correlations over more than three bonds.

(20) *Meta* couplings are *four*-bond correlations, which are often observed between aromatic protons residing on the same ring in *meta* positions with respect to each other, due to the efficient conjugation in the aromatic ring.

(21) A heteronuclear multiple-bond coherence experiment (HMBC) is used to reveal mainly three-bond correlations between carbons and protons.

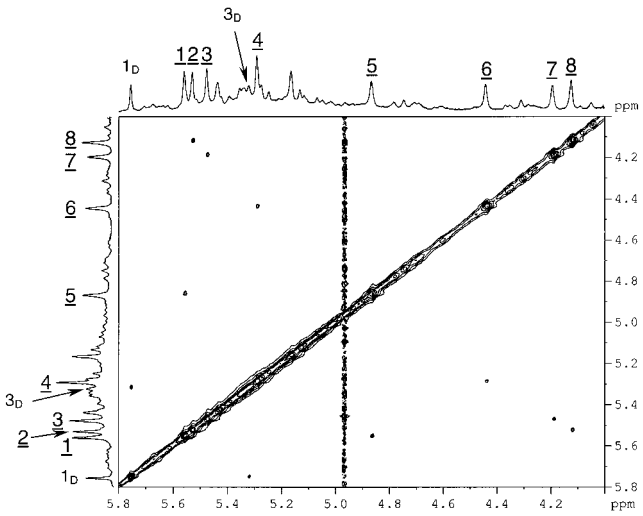

Figure 4. Portion of the total correlation (TOCSY) spectrum (at 250 K) of the dimer and tetramer of **2**$^{4-}$, showing *four*-bond ^{1}H−^{1}H correlations distinguishing four pairs of aromatic protons which correspond to four types of aromatic rings existing in the tetramer (two in each type of layer). The additional correlation observed is attributed to the dimer (which peaks are labeled with smaller font size and a subscript D).

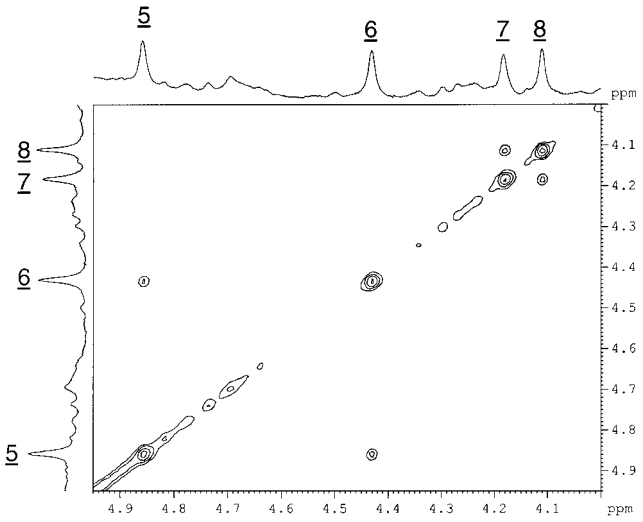

Figure 5. Portion of the NOESY spectrum (at 250 K) of the tetramer of **2**$^{4-}$, showing two through-space correlations identifying the more crowded biphenyl-type bay protons (no other NOE correlations are observed between the other aromatic protons).

Relatively strong through-space (nuclear Overhauser effect, NOE) correlations evidence spatial proximity between 5↔6 and 7↔8 (Figure 5). These unexpected correlations[22] are naturally assigned to the more crowded biphenyl-type bay, which apparently lost their symmetry. Thus the most upfield "aromatic" protons (of the type 5, 6, 7, and 8) are identified as the biphenyl-type bay protons (H-3 type in the parent compound). On the basis of this spectrum, the four pairs identified in the TOCSY spectrum are attributed to *two types* of **2**$^{4-}$ components, as through-*bond* correlations (both homonuclear and heteronuclear) between the nuclei of one component to the nuclei of the other component are absent. These two types of components, assumed to be layers in an aggregate (following the dimer observation), were named P and Q (see Figure 6A).

(22) In the parent compound no NOE correlations are observed between the aromatic protons due to the fact that the bays in it are symmetrical.

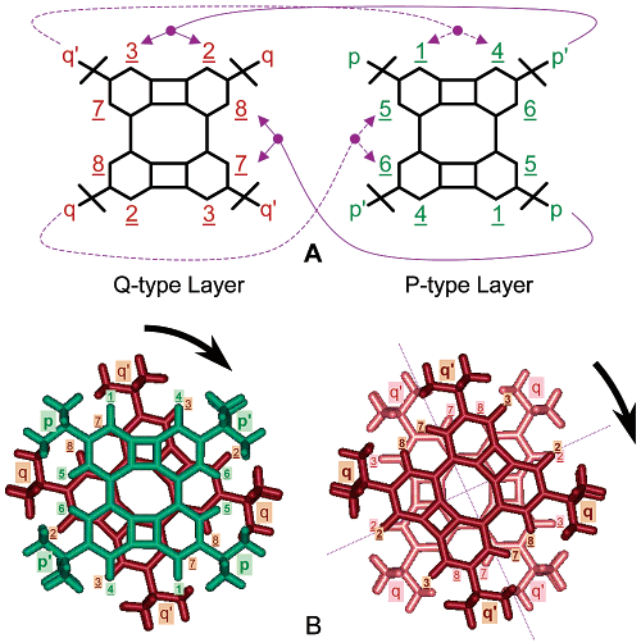

Figure 6. (A) Some key through-space correlations observed between the P-type and Q-type layers in the helical tetramer of $\mathbf{2}^{4-}$. (B) Mode of stacking of each two adjacent layers. Layers P_1, Q_1, and Q_2 are colored green, red, and light red, respectively. Numbering is according to Figure 1B; front layer labels are in boldface. Arrows show the helical turn when going from top downward: (left) P_1-Q_1 and (right) Q_1-Q_2. Dotted lines denote the two C_2 axes of symmetry that render the two inner layers (Q_1 and Q_2) symmetrically equivalent, as well as rendering the two outer layers (P_1 and P_2) symmetrically equivalent.

Table 1. Key Through-Space Correlations between the *tert*-Butyl Groups and the "Aromatic" Protons in the Tetramer of $\mathbf{2}^{4-}$, Identifying Its Structure as a Helical Tetramer

	intramolecular	intermolecular	
p	1,5	7,8	
p′	4,6	2,3	
q	2,8	5,6	3,2
q′	3,7	1,4	8,7

Further long-range $^{13}C-^{1}H$ correlations completed the assignment of the "aromatic" protons in the two types of layers in terms of local C_2 symmetry (Figure 6A, for a detailed description and completion of the NMR spectra assignment see the Supporting Information, Figures S2 and S3). This assignment indicates that both bisecting planes of reflection existing in the neutral **2** and its dianion are absent in the aggregated structure, and only the principle C_2 axis is retained. Therefore, the P and Q layers are stacked one *on top* of the other rather than in a stair-like arrangement.

The key evidence for the helical tetramer is obtained from the through-space correlations between the *tert*-butyl groups and the "aromatic" protons (Table 1, for the ROESY spectrum see the Supporting Information[23]). In addition to the expected intramolecular NOE correlations between each *tert*-butyl group and its adjacent "aromatic" protons attached to the same six-membered ring, other correlations are observed,[23] in which each *tert*-butyl group of one layer correlates to a selected couple of bay protons of the other type of layer. These correlations demonstrate the helical stacking of the two types (P with Q) of

(23) Figure S4 of the Supporting Information.

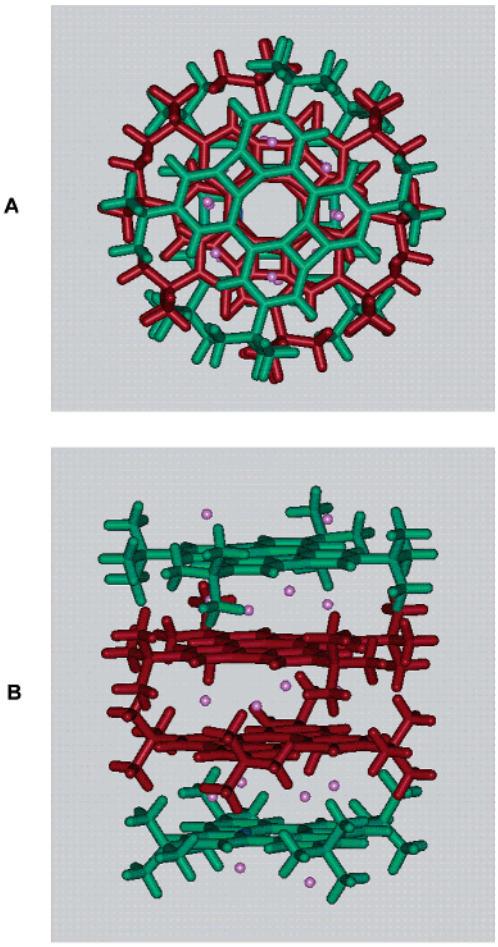

Figure 7. Computer-generated illustrations of the helical structure of $(\mathbf{2}^{4-})_4 \cdot 16Li^+$: (A) top view and (B) side view.

layers (Figure 6). The Q-type layers show, however, two additional correlations (q↔3 and q′↔8)[23] that seem impossible to be intramolecular (see Figure 6A). Therefore these two correlations must originate from two helically stacked Q-layers (Figure 6B), in which the additional correlations observed are identified as *inter*molecular (rather than intramolecular) interactions, analogously to the way that the stacking between the P and Q layers is deduced.[24] This implies that this species is a tetramer of $\mathbf{2}^{4-}$ units, consisting of four stacked layers P−Q−Q−P with a helical arrangement between each two adjacent layers. According to the NOE correlations, the helical turn from the P_1-Q_1 arrangement progresses in the same direction in the arrangement of the other layers (Figure 6B), thus forming an overall D_2-symmetric helix (Figure 7). In this structure, two C_2 symmetry axes reside on a plane that is perpendicular to the principal C_2 symmetry axis and located exactly between the two inner layers (Figure 6B). These axes render the two inner layers equivalent as well as rendering the two outer layers equivalent in the static, helical structure of the tetramer.

The P-layer and the Q-layer are therefore unequivocally identified as the outer and inner layers, respectively, of a helical tetramer. A fundamental difference between these two types of layers is that each inner layer is sandwiched between *two* tetraanionic layers, whereas each outer layer "senses" only one

(24) As each *tert*-butyl group should correlate to *two* bay protons lying above/below it, evidently the correlation signals observed for q↔2 and q′↔7 have contributions from the regular intramolecular interactions and the intermolecular interactions (Table 1).

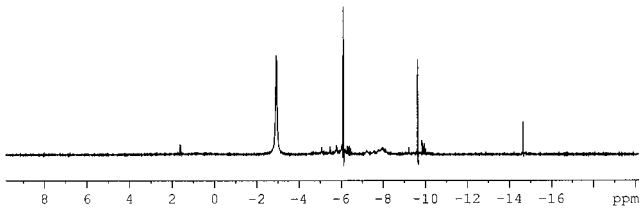

Figure 8. ^{7}Li NMR (acquired at 220 K) of a mixture of $\mathbf{2}^{2-}$ and $\mathbf{2}^{4-}$ dimer and tetramer exhibiting the ^{1}H NMR spectrum shown in Figure 1B. The broad peak at δ −2.1 is attributed to solvent-separated lithium cations, and the other dominant peaks are attributed to the tetraanion tetramer. The smaller peaks are attributed to the tetraanion dimer, and other aggregated modes existing in residual amounts.

layer in its close vicinity. Therefore the nuclei of the inner layers should be most affected by ring currents as compared to their counterparts in the outer layers.[25] In general, nuclei located close to the tetramer's principal C_2 axis (e.g., the "aromatic" protons) should be shielded by aromatic ring currents whereas groups extending to the outside of the structure (i.e., the *tert*-butyl groups) should be in the deshielding region. Indeed, comparison between the chemical shift values of analogous protons in the outer and inner layers shows that the "aromatic" protons of the inner layers are more shielded than their counterparts in the outer layers (H-4 being the only exception). Consistently, the *tert*-butyl groups of the inner layers are more *deshielded* than the *tert*-butyl groups in the outer layers. Moreover, the ^{7}Li NMR spectra of mixtures of the dianion of **2** and aggregates of $\mathbf{2}^{4-}$ show peaks with unprecedented high-field chemical shift values of $\delta < -14.5$ ppm (Figure 8).[26] Such peaks are absent in solutions containing only the dianion of **2**. This indicates that some lithium cations are present in a highly shielded environment, hinting at their possible location within the tetramer structure as sandwiched between the PAH decks in the shielding region of the mutually reinforcing ring currents of several aromatic decks. The shielding/deshielding effects observed on the different types of nuclei do not only support the structural assignment but also account for the aromatic character of $\mathbf{2}^{4-}$, and act as evidence, as well, for the role of the lithium cations as the electrostatic glue attracting the mutually repelling, negatively charged hydrocarbon layers.

Quantitative structural information is obtained by integrating the NOE correlation peaks observed in a ROESY[27] spectrum. Especially informative are the effective "diagonal" distances between the clashing *tert*-butyl groups of the outer (P) and inner (Q) layers that are measured from the respective ROESY correlation peaks. Four types of separation distances exist: a long one (6.0 ± 0.5 Å, between p′↔q′), a short one (3.8 ± 0.5 Å, between p↔q) and two equal distances of medium value (4.5 ± 0.5 Å, between p↔q′ and p′↔q). Since in each layer the *tert*-butyl groups are located at the corners of a virtual rectangle, the "diagonal" distances can be envisioned as the distances between each pair of adjacent corners of two rectangles, which are stacked with a phase angle between them. To obtain the three types of distances measured in the ROESY spectrum the two rectangles must lie one on top of the other with an approximately 45° phase, which is therefore determined as the experimental phase angle between the outer and inner layers. Assigning the correlations to the respective *tert*-butyl groups reproduces the correct direction of elongation of the BPD moiety as well.[14] The interlayer distances are obtained with the help of semiempirical MNDO (modified neglect of diatomic overlap) molecular orbital calculations,[28] based upon the tetramer structures having four lithium cations between each pair of adjacent layers, which showed a good correlation with the experimental NOE-effective proton−proton distances. The phase angle and distance calculated between the outer−inner pair are 44.3 ± 0.5° (as expected) and 4.2 ± 0.5 Å, respectively, whereas between the inner−inner pair a 42.5 ± 0.5° phase angle and a 4.3 ± 0.5 Å distance are calculated.

At a first glance, it seems peculiar that the interlayer distance in the tetraanionic tetramer $\mathbf{2}^{4-}$, where electrostatic repulsion prevails, is very similar to the interlayer distance of the neutral crystalline **2**.[14] Although the phases of the two systems are different, the tight association of the Li^{+} ions in the interlayer structure could provide a mechanism for the mutual attraction of the negatively charged layers.

Helically Stacked Structure of a Trimer of $\mathbf{2}^{4-}$ and Mechanistic Implications. The other identified species is attributed to a helical trimer of $\mathbf{2}^{4-}$. It shows a 6-fold multiplication of the ^{1}H NMR spectral pattern (vs the parent compound), which is consistent with three types of layers arranged in C_2 symmetry (Figure 1C). Its NOE pattern unequivocally establishes its helical structure, analogously to the structure determination of the tetramer (for the 2D NMR spectra see the Supporting Information). Magnetic shielding/deshielding effects show the same trend observed in the tetramer; the inner layer (identified as the only one showing through-space correlations to both other layers) is the most influenced by the other layers' aromatic currents, and is easily distinguished from the other layers by means of chemical shifts.

The trimer peaks build up at the expense of the dimer peaks in the early stages of the dimer formation (when the solution still contains predominately dianion, and is under reduction conditions at low temperature). The trimer appearance is immediately followed by the tetramer evolution. The trimer is by far the most elusive one, as it is the first to be consumed when the solution is warmed to room temperature. This leads to the suggestion that the tetramer can be formed by two main mechanisms (eqs 1 and 2):

$$\text{dimer} + \text{dimer} \rightleftharpoons \text{tetramer} \qquad (1)$$

$$\text{trimer} + \text{trimer} \rightleftharpoons \text{tetramer} + \text{dimer} \qquad (2)$$

The second mechanism (eq 2) resembles a redox disproportionation of two radical trianions to a dianion and a tetraanion, which was proposed as the reduction pathway for corannulene.[29]

On the basis of our previously described observations, the trimer formation itself requires the presence of dianions under reduction conditions along with already formed dimers. In this way, a freshly generated tetraanion monomer associates with existing dimers to form the trimer.

(25) Similar phenomena were observed in other PAH aggregates, for example: Ochsenfeld, C.; Brown, S. P.; Schnell, I.; Gauss, J.; Spiess, H. W. *J. Am. Chem. Soc.* **2001**, *123*, 2597−2606.

(26) To our knowledge the highest shielding effect on lithium cations was recorded for lithium biscyclopentadienide.[12a]

(27) Rotating frame Overhauser Effect Spectroscopy. The integrals of the through-space correlation peaks obtained in a quantitative ROESY experiment (using short mixing time delays) are proportional to the number of interacting protons and the average inverse sixth power of the inter-proton distances.

(28) (a) Dewar, M. J. S.; Thiel, W. *J. Am. Chem. Soc.* **1977**, *99*, 4899. (b) Thiel, W. *Quantum Chemistry Program Exchange*; Indiana University: Bloomington, IN, 1982; Vol. 2, No. 438, p 63.

Self-Diffusion Measurements.[30] Self-diffusion rate constants measured at 259.6 K for the $\mathbf{2}^{4-}$ tetramer, trimer, dimer, and $\mathbf{2}^{2-}$ (monomer), all present simultaneously in the same solution mixture (hence the measurement was carried out under the same conditions for all species), are 2.5(±0.1), 2.7(±0.1), 3.1(±0.3), 3.8(±0.2) × 10^{-10} m^2 s^{-1}, respectively. Self-diffusion measurements of the ^{7}Li signals attributed to the dimer and the tetramer yield rate constant values similar to those obtained from the measurements of the respective ^{1}H signals, supporting the ^{7}Li NMR assignment.

The Stokes−Einstein equation, $D = k_BT/6\pi\eta r$, inversely relates the self-diffusion rate constant D of a rigid spherical particle to its radius r (k_B is Boltzmann constant, T is temperature, and η is viscosity). The tetraanionic aggregates under consideration are far from being spherical, and approximating their shape to oblate spheroids seems a realistic model. Spheroids have greater surface area than spherical particles of the same volume, hence they exhibit larger frictional coefficients. The denominator in the Stokes−Einstein equation, which stands for the frictional coefficient, is therefore corrected by multiplication with Perrin[30f] factors (F) for each aggregation mode. The Perrin factors are calculated from the ratio between the long and short semi-axes,[30f] which is assumed to grow linearly with the number of layers (n). On the basis of the MNDO calculations we estimate 4.0 Å for the monomer's thickness (which is approximately equal to the interlayer spacing in the aggregate, and also accounts for solvation effects[31]) and 15.6 Å for the monomer's diagonal. These measures were taken as the spheroid's short and long diameters, respectively. According to the approximation of a linear growth of the aggregate's volume with the number of layers, we derive the following relation from the modified Stokes−Einstein equation:

$$D = \frac{k_BT}{6\pi\eta rF} = \frac{k_BT}{6\pi\eta(3V/4\pi)^{1/3}F} = \frac{k_BT}{6\pi\eta(3V_0\cdot n/4\pi)^{1/3}F} \quad (3)$$

where V is the volume of the aggregate (which is equal to the volume of the sphere corresponding to the radius r)[32] and V_0 is the volume of the monomer. Plotting the measured rate constants (D) against $1/(n^{1/3}\cdot F)$ yields a straight line ($R^2 = 0.98$), which from its slope is calculated an effective monomer volume (V_0) of ca. 520 Å^3. This value perfectly matches the MNDO-based estimation of the monomer's effective dimensions.

Conclusions and Outlook

A dimer, a trimer, and a tetramer of $\mathbf{2}^{4-}$, all self-assembled in helically stacked structures, have been observed and fully characterized in solution by NMR spectroscopy. Magnetic shielding effects and self-diffusion measurements support the structural features of the resulting supramolecular structures. Each two adjacent layers are separated by slightly over 4 Å, which leaves the appropriate spacing for lithium cations to intercalate between the layers. The clashing between the bulky *tert*-butyl groups, locked in a gear-meshed structure, yields the helical relation between each two adjacent layers. Other arrangements of the tetramer that retain this relation and are *not* helical (e.g., a zigzag arrangement) contradict the NOE pattern observed. Apparently, eclipsed relations even between nonadjacent layers, which exist in the other arrangements of this sort, disfavor these arrangements over the helical structure.

The failure to detect the monomer of $\mathbf{2}^{4-}$ and the tendency to favor the high-order aggregates[33] reveal that this phenomenon is an important feature of highly charged PAHs. The geometrical structure of BPD points at a similarity between the aggregates of BPD and aggregates of other PAHs reported in the literature[11−13] in terms of the planarity of the conjugated skeleton.[34] The fixed planar geometry of the charged decks in BPD derivatives apparently facilitates the formation of higher aggregates than a dimer, as was generally predicted previously.[13] This could serve as a guideline in the search for other suitable PAHs that would exhibit ionic aggregation in highly reduced states.

Experimental Section

General Procedures. THF-d_8 (Deutero GmbH) was dried over sodium−potassium alloy under vacuum. Lithium (Aldrich) was kept in paraffin oil and was rinsed shortly before use with petroleum ether (bp 40−60 °C).

1D and 2D NMR spectra were recorded on a Bruker DRX-400 spectrometer equipped with a ^{2}H lock and a BGUII z-gradient coil. The THF-d_7 low-field proton band was used for calibration of the ^{1}H NMR spectra (δ 3.575); the THF-d_8 ^{13}C low-field signal served for calibration of the ^{13}C NMR spectra (δ 67.393); the ^{7}Li NMR reference was 0.05 M LiBr in THF.

UV−vis absorption spectra were recorded at ambient temperature in a 2 mm path length quartz cell with a Perkin-Elmer Lambda 6 spectrophotometer. The quartz cell was equipped with high-vacuum PTFE stopcocks (Kontes). The spectrophotometer sample chamber was accessible from a Vacuum Atmospheres glovebox.

MNDO calculations were performed with MOPAC 93 (Fujitsu) software, with lithium parametrization taken from MNDOC.[28]

Preparation of the Reduction Samples. A lithium wire was freshly produced and directly inserted into the upper part of an extended NMR tube, which was previously filled with argon and contained the material (3−10 mg). The sample was attached to a vacuum line and flame-dried under vacuum. Dry THF-d_8 (ca.0.5 mL) was distilled from a reservoir to the tube. The sample was degassed under vacuum using the freeze−pump−thaw technique and flame-sealed.

(29) Baumgarten, M.; Gherghel, L.; Wagner, M.; Weitz, A.; Rabinovitz, M.; Cheng, P.-C.; Scott, L. T. *J. Am. Chem. Soc.* **1995**, *117*, 6254−6257. The redox disproportionation mechanism may as well be the reduction pathway here, since the tetraanions' peaks evolve concomitantly with the decrease in the dianion peak intensities. Presence of radical trianions in substantial amounts is not likely, since only a single set of isosbestic points is observed when the tetraanions are converted to dianions in the UV−vis titration experiment mentioned earlier in the text. Moreover, the spectra of both the dianion and the tetraanion remains sharp (typical half-width of 5−6 Hz) during either reduction of the dianions to tetraanions or oxidation (with the neutral compound) of the tetraanions to dianions.

(30) (a) Stejskal, E. D.; Tanner, J. E. *J. Chem. Phys.* **1965**, *42*, 288−292. (b) Tanner, J. E. *J. Chem. Phys.* **1970**, *52*, 2523−2526. (c) Stilbs, P. *Prog. Nucl. Magn. Reson. Spectrosc.* **1987**, *19*, 1−45. (d) Johnson, C. S. *Prog. Nucl. Magn. Reson. Spectrosc.* **1999**, *34*, 203−256. (e) For measurements of anions see: $\mathbf{2}^{4-}$: Cohen, Y.; Ayalon, A. *Angew. Chem., Int. Ed. Engl.* **1995**, *34*, 816−818. (f) Cantor, C. R.; Schimmel, P. R. *Biophysical Chemistry*; W. H. Freeman: San Francisco, 1980; Vol. 2, Chapter 10, pp 560−562.

(31) Hoffman R. E.; Shabtai, E.; Rabinovitz, M.; Iyer, V. S.; Müllen, K.; Rai, A. K.; Scott, L. T. *J. Chem. Soc., Perkin Trans. 2*, **1998**, 1659−1664.

(32) In the corrected Stokes−Einstein equation, r stands for the radius of a sphere having the same volume as the spheroid.

(33) After a long time under reduction conditions almost no dimer and trimer can be detected. Moreover, the tetramer is not dissociated to dimers even when the solution is considerably diluted, which is apparently due to the low concentrations used, but also hints to large equilibrium constants for the mechanisms shown in eqs 1 and 2.

(34) The bowl-shape of corannulene is considerably flattened at the tetraanionic stage (where dimerization occurs): (a) Sygula, A.; Rabideau, P. W. *J. Mol. Struct. (THEOCHEM)* **1995**, *333*, 215−226. (b) Sato, T.; Yamamoto, A.; Yamabe, T. *J. Phys. Chem. A* **2000**, *104*, 130−137.

Reduction Procedure. The solution was brought into contact with the lithium wire by turning the tube upside down at low temperatures (usually at −30 °C). Returning the sample to the upright position separated the solution from the metal wire, thus stopping the reduction from progressing.

Oxidation Reactions. Two types of oxidation reactions were performed to show the reversibility of the reduction process: (a) with oxygen, to yield the neutral compound and (b) with the neutral compound in equivalent amount, to yield to dianion (and thus to establish the reduction state as the tetraanion). The oxygenation reactions were carried out by opening the samples under anhydrous conditions and blowing the gas via a syringe into the tube. The deep color of the anions gradually disappeared and the ^{1}H NMR spectra were recorded. The reaction with the neutral compound was performed in the following way. Equivalent amounts of the material were introduced to an extended, breakable ampule and an NMR tube with a 14-mm-diameter extension pipe. The ampule was attached to the vacuum line, flame-dried under vacuum, and flame-sealed. The closed ampule was inserted into the extension of the NMR tube along with a glass piece, serving as a "hammer". A regular 8-mm-diameter extension pipe was attached to the upper part of the sample by glass blowing. The preparation of the sample (insertion of the lithium wire, solvent distillation, etc.) was then completed as usual. After the material in the tube has completely transformed into the tetraanion, the hammer was used to break open the ampule, allowing the neutral material to mix with the tetraanionic solution. The ^{1}H NMR spectra of the resulting mixture were recorded before and after this operation (see Supporting Information).

Self-Diffusion Measurements.[30] The self-diffusion measurements were performed at different reduction stages with use of a modified pulsed field gradient stimulated spin−echo technique.[35] The measurements were carried out in a sealed extended 4-mm-diameter Pyrex tube inserted into a regular 5-mm-diameter NMR tube (to avoid convection due to sample heating by the RF pulses). A small amount of benzene was introduced to the sample to serve as an internal reference for viscosity changes. The rate constant measured for benzene from the dianion state onward was 1.48 (±0.2) × 10^{-9} m^2 s^{-1}, independent of the solute composition once **2** was totally converted to its dianion. The pulsed gradient strengths used were in the range 1.7−32.3 G cm^{-1}, and their duration and the time between the start of the first gradient pulse and the start of the second were 5 and 50 ms, respectively. The diffusion coefficient calculated for each species is an average of the values obtained for each peak attributed to that species. Only data having a correlation coefficient (R^2) of more than 0.998 were included.

Synthesis of 2,5,8,11-Tetraisopropylcycloocta[1,2,3,4-*def*;5,6,7,8-*d′e′f′*]bisphenylene (3). The synthesis followed the previously published route to cycloocta[1,2,3,4-*def*;5,6,7,8-*d′e′f′*]bisphenylenes.[14] Orange powder, mp 258−258.5 °C. Anal. Calcd for $C_{36}H_{36}$: C, 92.26; H, 7.74. Found: C, 91.83; H, 7.79. HREI-MS cluster: *m*/*z* (% RA for *m*/*z* =50−490): 469.2864 ([M + 1]$^+$, 39%, −2.8 ppm for $^{13}C_1$ $^{12}C_{35}{}^1H_{36}$), 468.2821 (M^+, 100%, −0.8 ppm for $^{12}C_{36}{}^1H_{36}$), 453.2598 ([M − CH_3]$^+$, 16%, −3.4 ppm for $^{12}C_{35}{}^1H_{33}$). IR (cm^{-1}, C−H stretch region): 3049, 2953, 2924, 2896, 2864.

Computational Details. To avoid elaborate calculations we fixed the conjugated skeleton of each layer in a flattened rigid conformation, allowing only the principle physical forces that govern the aggregate structure (e.g., the electrostatic forces between the charged layers and the lithium cations) to be expressed.

The interatomic distances and angles for the layers were taken from the minimum-energy structure of the monomer of $\mathbf{2}^{4-}$, found by Density Functional Theory calculations (at B3LYP/6-31G* level of theory). The energy difference between the planar structure and the minimum-energy structure is less than 0.5 kcal mol^{-1}.

(35) Wu, D.; Chen, A.; Johnson, C. S. Jr. *J. Magn. Reson. A* **1995**, *115*, 260−264.

The partial optimization of different arrangements of the tetramer structure of $\mathbf{2}^{4-}$ was restricted to the interlayer distances and dihedral phase angles, liberating also the lithium cations and the rotation of the substituent groups. All possible arrangements of the lithium cations within the D_2 symmetry group were calculated.

NOE-effective proton−proton distances obtained from the calculated structure show 90% correlation (*R* value) to the experimentally measured effective distances; 99% correlation is observed for the four types of key "diagonal" *tert*-butyl−*tert*-butyl distances.

NMR Data. 1: δ_H (THF-d_8, 298 K) 6.33 (H-1, d, J = 6.8 Hz, 4 H), 6.57 (H-2, dd J_1 = 8.6 Hz J_2 = 6.8 Hz, 4 H), 6.81 (H-3, d, J = 8.5 Hz, 4 H) ppm. δ_C (THF-d_8, 298 K) 117.81 (C-1), 124.14 (C-3), 126.65 (C-3a), 130.64 (C-2), 150.18 (C-6c), 151.84 (C-6a) ppm.

$\mathbf{1}^{2-}$/2Li$^+$: δ_H (THF-d_8, 250 K) ^{1}H: 5.72 (H-1, d, J = 5.4 Hz, 4 H), 5.90 (H-2, dd, J_1 = 8.9 Hz, J_2 = 5.4 Hz, 4 H), 7.56 (H-3, d, J = 8.9 Hz, 4 H) ppm. δ_C (THF-d_8, 250 K) 97.03 (C-1), 101.28 (C-3a), 109.80 (C-2), 123.08 (C-3), 125.58 (C-6c), 153.12 (C-6a) ppm. δ_{Li} (THF-d_8, 250 K) −2.7 (broad), −9.6, −13.0 ppm (the two peaks at high field are attributed to ca. 2% of dissolved tetraanionic aggregated structures).

2: δ_H (THF-d_8, 298 K) 1.22 (Me, s, 36 H), 6.49 (H-1, d, J = 1.2 Hz, 4 H), 6.77 (H-3, d, J = 1.2 Hz, 4 H) ppm. δ_C (THF-d_8, 298 K) 31.02 (Me), 35.79 (^{t}Bu), 116.06 (C-1), 118.88 (C-3), 125.93 (C-3a), 147.46 (C-6c), 151.57 (C-6a), 153.41 (C-2) ppm.

$\mathbf{2}^{2-}$/2Li$^+$: δ_H (THF-d_8, 220 K) 1.40 (Me, s, 36 H), 5.84 (H-1, s, 4 H), 7.50 (H-3, s, 4 H) ppm. δ_C (THF-d_8, 220 K) 32.34 (Me), 35.76 (^{t}Bu), 95.10 (C-1), 99.16 (C-3a), 115.60 (C-3), 123.70 (C-6c), 130.59 (C-2), 152.47 (C-6a) ppm. δ_{Li} (THF-d_8, 220 K) −3.1 ppm.

$\mathbf{2}^{4-}$/4Li$^+$: In the low-symmetry aggregates of $\mathbf{2}^{4-}$ an apostrophe denotes the second type of substituted benzene ring within each layer, according to the local C_2 symmetry.

($\mathbf{2}^{4-}$/4Li$^+$)$_2$ (dimer): δ_H (THF-d_8, 240 K) 1.63 (Me, s, 72 H), 5.31 (H-3, s, 8 H), 5.73 (H-1, s, 8 H) ppm. δ_H (THF-d_8, 180 K) 1.53 (Me, s, 36 H), 1.63 (Me′, s, 36 H), 5.05 (H-3, s, 4 H), 5.46 (H-3′, s, 4 H), 5.65 (H-1, s, 4 H), 5.73 (H-1′, s, 4 H) ppm. δ_C (THF-d_8, 240 K) 34.12 (Me), 36.52 (^{t}Bu), 67.5 (C-3), 81.93 (C-1), 84.77 (C-6c), 97.00 (C-3a), 97.57 (C-6a), 124.57 (C-2) ppm. δ_{Li} (THF-d_8, 200 K) complex spectrum, major peaks: −4.7, −5.6, −7.2, −7.7 ppm. Each of the last two pairs of peaks coalesces at higher temperatures to yield two bands of roughly 1:1 integration ratio.

($\mathbf{2}^{4-}$/4Li$^+$)$_3$ (trimer): δ_H (THF-d_8, 220 K) "Top" layer, 1.55 (Me, s, 18 H), 1.57 (Me′, s, 18 H), 4.56 (H-3, s, 2 H), 4.85 (H-3′, s, 2 H), 5.26 (H-1, s, 2 H), 5.46 (H-1′, s, 2 H); Middle layer, 1.89 (Me, s, 18 H), 1.91 (Me′, s, 18 H), 4.44 (H-3′, s, 2 H), 4.59 (H-3, s, 2 H), 5.65 (H-1, s, 2 H), 5.67 (H-1′, s, 2 H); "Bottom" layer, 1.56 (Me, s, 18 H), 1.60 (Me′, s, 18 H), 4.56 (H-3, s, 2 H), 5.05 (H-3′, s, 2 H), 5.43 (H-1, s, 2 H), 5.67 (H-1′, s, 2 H) ppm.

($\mathbf{2}^{4-}$/4Li$^+$)$_4$ (tetramer): [labeling according to the text (Figure 1B) is attached in braces]: δ_H (THF-d_8, 250 K) Outer (P-type) layers, 1.47 (Me′ {p′}, s, 36 H), 1.50 (Me {p}, s, 36 H), 4.43 (H-3′ {6}, s, 4 H), 4.86 (H-3 {5}, s, 4 H), 5.28 (H-1′ {4}, s, 4 H), 5.55 (H-1 {1}, s, 4 H); Inner (Q-type) layers, 1.75 (Me′ {q′}, s, 36 H), 1.81 (Me {q}, s, 36 H), 4.11 (H-3 {8}, s, 4 H), 4.18 (H-3′ {7}, s, 4 H), 5.47 (H-1′ {3}, s, 4 H), 5.52 (H-1 {2}, s, 4 H) ppm. δ_C (THF-d_8, 250 K) [for simplicity, carbons in each of the two types (according to the local C_2 symmetry) of substituted benzene ring within each layer are numbered sequentially C-1...C-6/C-1′...C-6′, where enumeration of positions 1...3 (and similarly 1′...3′) coincides with the enumeration in the parent compound]: Outer (P-type) layers, 34.04 (Me′), 34.40 (Me), 35.74 (^{t}Bu′), 36.04 (^{t}Bu), 59.52 (C-3′), 66.64 (C-3), 81.52 (C-5′), 81.60 (C-5), 82.17 (C-1′), 83.38 (C-1), 92.55 (C-6), 96.14 (C-4), 96.57 (C-4′), 100.70 (C-6′), 122.65 (C-2′), 124.15 (C-2); Inner (Q-type) layers, 33.93 (Me), 34.09 (Me′), 36.11 (^{t}Bu), 36.34 (^{t}Bu′), 59.26 (C-3), 61.53 (C-3′), 75.50 (C-5), 80.13 (C-5′), 83.90 (C-1′), 86.62 (C-1), 89.79 (C-6′), 91.55 (C-4′), 91.90 (C-4), 95.36 (C-6), 122.91 (C-2), 130.50 (C-2′) ppm. δ_{Li} (THF-d_8, 220 K) 1.6, −6.1, −9.6, −14.7 ppm.

3: δ_H (THF-d_8, 298 K) 1.14 (Me, d, $J = 6.9$ Hz, 24 H), 2.60 (^{i}Pr, m, $J = 6.9$ Hz, 4 H), 6.28 (H-1, s, 4 H), 6.63 (H-3, s, 4 H) ppm. δ_C (THF-d_8, 298 K) 23.68 (Me), 35.75 (^{i}Pr), 116.22 (C-1), 121.15 (C-3), 126.19 (C-3a), 147.91 (C-6c), 151.28 (C-2), 151.69 (C-6a) ppm.

3^{2-}/2Li$^+$: δ_H (THF-d_8, 220 K) 1.30 (Me, d, $J = 6.7$ Hz, 24 H), 2.82 (^{i}Pr, m, $J = 6.6$ Hz, 4 H), 5.62 (H-1, s, 4 H), 7.32 (H-3, s, 4 H) ppm. δ_C (THF-d_8, 220 K) 25.43 (Me), 37.31 (^{i}Pr), 94.62 (C-1), 99.13 (C-3a), 118.06 (C-3), 124.70 (C-6c), 128.97 (C-2), 152.75 (C-6a) ppm. δ_{Li} (THF-d_8, 220 K) −2.9 ppm.

(3^{4-}/4Li$^+$)$_2$ (dimer): δ_H (THF-d_8, 250 K) 1.48 (Me_1, d, $J = 6.7$ Hz, 24 H), 1.55 (Me_2, d, $J = 6.7$ Hz, 24 H), 3.19 (^{i}Pr, m, $J = 6.7$ Hz, 8 H), 5.15 (H-3, s, 8 H), 5.69 (H-1, s, 8 H) ppm. δ_C (THF-d_8, 250 K) 25.84 (Me_2), 27.06 (Me_1), 36.79 (^{i}Pr), 70.11 (C-3), 82.39 (C-1), 84.97 (C-6c), 97.77 (C-3a), 97.77 (C-6a), 121.84 (C-2) ppm. δ_{Li} (THF-d_8, 200 K) complex spectrum, major peaks: −6.6, −8.0, −10.3, −13.7, −15.0, −15.2, −15.7, −16.5 ppm. Shows a dynamic process analogous to the ^{7}Li NMR spectra of the dimer of $\mathbf{2}^{4-}$, and absorption bands at similar frequencies as the aggregated species of $\mathbf{2}^{4-}$.

Acknowledgment. We are indebted to Prof. Klaus Müllen and Prof. Yoram Cohen for helpful discussions and suggestions. We thank Dr. Ronald Beust, Dr. David Danovich, and Ms. Shari Damast for assistance in the calculations, and Dr. Suchada Rajca for the UV−vis titration experiment and graphical illustrations. Financial support from the US-Israel Binational Science Foundation (BSF), the National Science Foundation (CHE-9806954), and the Lise Meitner-Minerva Center for Computational Quantum Chemistry is gratefully acknowledged.

Supporting Information Available: Symmetry analysis of **2**; proof of local C_2 symmetry in the tetramer units; HMBC and ROESY spectra of $\mathbf{2}^{4-}$ tetramer; two-dimensional NMR spectra of $\mathbf{2}^{4-}$ trimer establishing its helical structure; and NMR oxidation experiment of $\mathbf{2}^{4-}$ and UV−vis titration experiment (PDF). This material is available free of charge via the Internet at http://pubs.acs.org.

JA012140U